Functional Segmentation of Dynamic Emission Tomographic Images

Koon-Pong Wong[1,2] **Dagan Feng**[2,3] **Steven R. Meikle1** **Michael J. Fulham**[1,4]

[1]Department of PET and Nuclear Medicine, Royal Prince Alfred Hospital, Camperdown, NSW 2050, Australia
[2]Basser Department of Computer Science, The University of Sydney, NSW 2006, Australia
[3]Department of Electronic and Information Engineering, The Hong Kong Polytechnic University, Hong Kong
[4]Faculty of Medicine, The University of Sydney, NSW 2006, Australia

kpong@cs.usyd.edu.au

Abstract

Emission tomography such as positron emission tomography (PET) and single-photon emission computed tomography (SPECT) can provide *in vivo* measurements of dynamic physiological and biochemical processes in humans. A limitation of both PET and SPECT is their inability to provide precise anatomic localisation due to relatively poor spatial resolution and high noise levels when compared to magnetic resonance (MR) imaging. Manual placement of regions of interest (ROIs) is commonly used in clinical and research settings in analysis of PET and SPECT data. However, this approach is operator dependent and time-consuming. Semi- or fully-automated ROI delineation (or segmentation) methods offer advantages by reducing operator error and subjectivity and thereby improving reproducibility. In this paper, we describe an approach to automatically segment dynamic PET images based on functional difference using cluster analysis, and we validate our approach with a simulated phantom study and assess its performance in segmentation of dynamic lung data. Our results suggest that cluster analysis can be used to automatically segment tissues in dynamic PET and SPECT studies.

Keywords: Segmentation, cluster analysis, positron emission tomography (PET).

1 Introduction

With nuclear medicine imaging modalities like PET and SPECT, we are able to study the functional or pathophysiological change in local tissues quantitatively by analysing the underlying tissue time-activity curves (TACs) extracted by manually putting regions of interest (ROIs) around those areas which are of interest. This approach, although is widely used in clinical and research settings, is not reproducible as it is operator dependent and time-consuming. In order to remove as much subjectivity as possible, semi- or fully-automated ROI delineation (or segmentation) methods would be desirable as the resultant ROIs are expected to be more reproducible. In this work, we describe an approach to automatically segment dynamic PET images using cluster analysis, and we validate it using a simulated dynamic 2-[^{11}C]thymidine PET study with a slice of Zubal phantom (Zubal *et al*., 1994).

2 Materials and Methods

2.1 Segmentation Scheme

The segmentation method is based on cluster analysis. Our aim is to classify a number of tissue TACs according to their shape and magnitude into a smaller number of distinct characteristic classes that are mutually exclusive so that the tissue TACs within a cluster are similar to each others but are dissimilar to those drawn from other clusters. The clusters (or clustered ROIs) represent the locations in the images where the tissue TACs have similar kinetics. The kinetics associated with a cluster (i.e. cluster centroid) is the average of TACs in the cluster. Suppose that there exists k characteristic curves in the dynamic PET data which has m tissue TACs each of which has n time frames with $k << m$ and that any tissue TAC belongs to only one of the k curves. The clustering algorithm then segments the dynamic PET data into k ROIs automatically based on a weighted Euclidean distance measure. There is no explicit assumption on the structures of data and the clustering proceeds automatically in an unsupervised manner. As the number of clusters, k, for a given data set is usually not known *a priori*, it is usually determined by trial and error. In addition, the initial cluster centroid in each cluster was initialised randomly to ensure that all clusters are non-empty. Each tissue TAC is then allocated to its nearest cluster centroid which is then updated according to the distance measure so that the latter is minimised. The above allocation and updating processes are repeated for all tissue TACs until there is no reduction in moving one tissue TAC from one cluster to the other cluster. On convergence, the cluster centroids are mapped back to the original data space for all pixels. An improved signal-to-noise ratio can be achieved because each pixel in the mapped data space is represented by one of the cluster centroids each of which possesses a higher statistical significance than an individual TAC.

2.2 Validation Study

To examine the validity of the segmentation scheme, a dynamic 2-[^{11}C]thymidine PET study was simulated. Typical 2-[^{11}C]thymidine kinetics for different tissues were derived from 8 patients. The data were acquired on an ECAT 931 scanner (CTI/Siemens, Knoxville, TN). Images were reconstructed using filtered back-projection (FBP) with a Hann filter cut off at the Nyquist frequency. ROIs were drawn over the PET images to obtain the tissue TACs in bone, bone marrow, blood pool, liver,

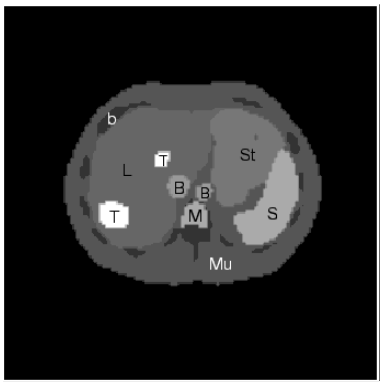

Figure 1: A slice of the Zubal phantom. B = blood vessels; b = bone; L = liver; M = marrow; Mu = muscle; S = spleen; St = stomach; T = tumour.

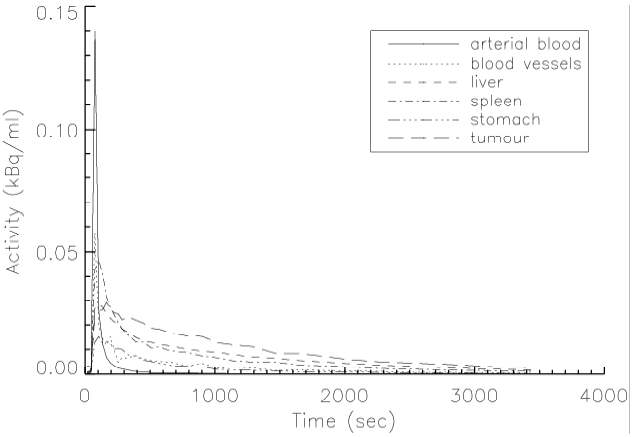

Figure 2: Simulated noisy 2-[^{11}C]thymidine kinetics in some representative regions. A metabolite-corrected arterial blood curve which was used to simulate 2-[^{11}C]thymidine kinetics in different tissues is also shown.

skeletal muscle, spleen, stomach and tumour. Impulse response functions (IRFs) corresponding to these tissues were determined by spectral analysis of the TACs (Cunningham and Jones, 1993). The average IRFs for each common tissue type were obtained by averaging the spectral coefficients across the subjects and convolved with a typical arterial input function, resulting in typical TACs for each tissue. The TACs were then assigned to the corresponding tissue types in a single slice of the Zubal phantom (Zubal *et al.*, 1994) which included blood vessels, bone, liver, bone marrow, muscle, spleen, stomach, a large and a small tumour in the liver (Figure 1), and a dynamic sequence of sinograms was obtained by forward projecting the images. Appropriate Poisson noise and blurring were also added to simulate realistic sinograms acquired on an ECAT 931 scanner. Noisy dynamic images were then reconstructed using FBP (Hann filter cutoff at the Nyquist frequency). Figure 2 shows the metabolite-corrected arterial blood curve and noisy 2-[^{11}C]thymidine kinetics in some representative tissues.

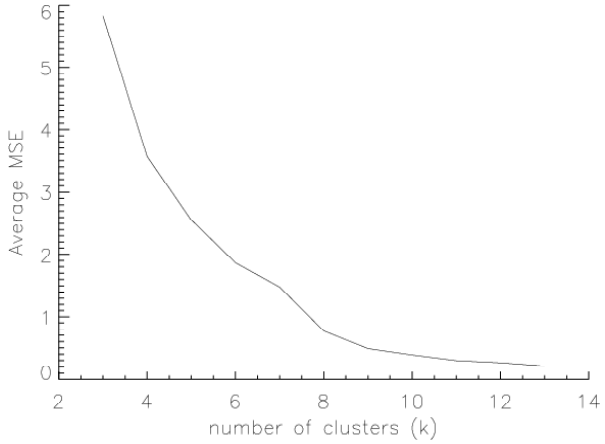

Figure 3: A slice of the Zubal phantom. B = blood vessels; b = bone; L = liver; M = marrow; Mu = muscle; S = spleen; St = stomach; T = tumour.

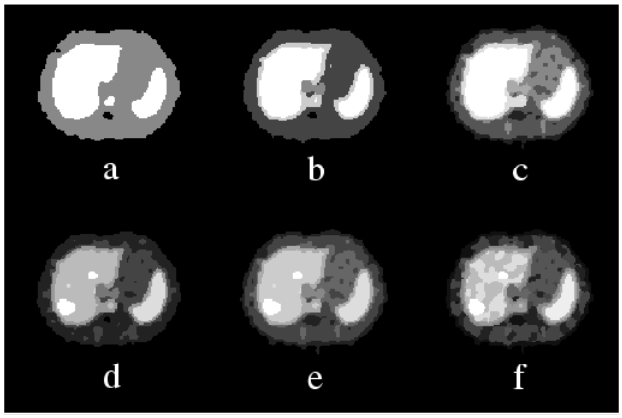

Figure 2: Simulated noisy 2-[^{11}C]thymidine kinetics in some representative regions. A metabolite-corrected arterial blood curve which was used to simulate 2-[^{11}C]thymidine kinetics in different tissues is also shown.

3 Results and Discussion

Figure 3 plots the average mean squared error (MSE) as a function of k. As shown in the figure, the average MSE decreases monotonically ($k < 8$), then decreases less rapidly ($8 \le k \le 9$) before reaching a plateau ($k \ge 10$). It demonstrated that 8 or 9 clusters can be used as a threshold to give convincing segmentation of the tissues.

Figure 4 shows the segmentation results using different number of clusters, k, in the clustering algorithm. The number of clusters is actually varied from 3 to 13 but only some representatives are shown. In each of the images in Figure 4, different grey levels are used to represent the cluster locations. It is seen that when the number of clusters is too small the segmentation of the data are not good. With $k = 3$, the liver, marrow and spleen are merged to form a cluster and the other regions are merged to form another cluster [Figure 4(a)]. With $5 \le k \le 7$ [Figures 4(b)-(c)], the segmentation results become better because the blood vessels and stomach are now visualised. However, the tumours cannot be identified while the liver and the spleen are still classified

into the same cluster because of the constraint on the value of *k*. With $k = 8$, the tumours are visualised and almost all of the regions are correctly identified [Figure 4(d)]. Increasing the value of *k* to 9 gives a slightly better segmentation [Figure 4(e)]. Further increasing the value of *k*, however, gives a poor segmentation because the actual number of tissues present in the data is less than the specified number of clusters, causing some homogeneous regions to be split [Figure 4(f)]. Thus, 8 or 9 clusters are enough to give reasonable segmentation of different tissues which agrees with the number of tissues present in the data.

4 Conclusions

In conclusion, we present an approach to segment tissues in dynamic PET images automatically using cluster analysis. Our results from a simulated PET study indicate that promising tissue segmentation can be achieved. We suggest that cluster analysis is useful to automatically segment tissues in dynamic PET studies and it may potentially replace manual ROI delineation which is operator dependent and time-consuming. The results obtained from this simulation study also encourage us to investigate the applicability of the approach to whole-body PET for lesion localisation and assessment of treatment response in a variety of oncological conditions.

5 Acknowledgements

This work was supported in part by the National Health and Medical Research Council (NHMRC) of Australia under grant 980042 and the University Grant Council (UGC) of Hong Kong.

6 References

CUNNINGHAM, V. J. and JONES, T. (1993): Spectral analysis of dynamic PET studies. *J. Cereb. Blood Flow Metab*. **13**:15-23.

ZUBAL, I. G., HARRELL, C. R., SMITH, E. O., RATTNER, Z., GINDI, G., and HOFFER, P. B. (1994): Computerized three-dimensional segmented human anatomy. *Med. Phys.* **21**:299-302.